Nuclear Inst. and Methods in Physics Research, A 890 (2018) 1–7

Contents lists available at ScienceDirect

Nuclear Inst. and Methods in Physics Research, A

journal homepage: www.elsevier.com/locate/nima

High gradient RF test results of S-band and C-band cavities for medical linear accelerators

A. Degiovanni *,[1], R. Bonomi [1], M. Garlasché [2], S. Verdú-Andrés [3], R. Wegner [2], U. Amaldi

TERA Foundation, via G.Puccini 11, 28100 Novara, Italy

ARTICLE INFO

Keywords:
Medical accelerators
Hadrontherapy
Cyclinac
Linac
RF cavity
Breakdown rate

ABSTRACT

TERA Foundation has proposed and designed hadrontherapy facilities based on novel linacs, i.e. high gradient linacs which accelerate either protons or light ions. The overall length of the linac, and therefore its cost, is almost inversely proportional to the average accelerating gradient. With the scope of studying the limiting factors for high gradient operation and to optimize the linac design, TERA, in collaboration with the CLIC Structure Development Group, has conducted a series of high gradient experiments. The main goals were to study the high gradient behavior and to evaluate the maximum gradient reached in 3 and 5.7 GHz structures to direct the design of medical accelerators based on high gradient linacs. This paper summarizes the results of the high power tests of 3.0 and 5.7 GHz single-cell cavities.

1. Introduction

The use of protons and light ions for the treatment of deep-seated solid tumors is spreading worldwide [1]. The field of hadrontherapy would benefit greatly from compact, efficient accelerators that make the setup and operation of a hadrontherapy facility more affordable. In this regard, high-gradient RF technology has the potential of providing more compact and efficient machines.

TERA Foundation has proposed and designed hadrontherapy facilities based on high-frequency linacs [2,3] and has developed acceleration scheme that combines a cyclotron used as injector with a high-gradient linac used as booster [4,5]. The largest contribution to the size of such systems comes from the last linac section. For example, 15–20 m-long linacs are typically needed for accelerating protons between 30 and 230 MeV, while a linac for carbon ions would be more than double in length. High accelerating gradients can be used in order to make the linac more compact and less expensive. However, such high gradients will result in large peak surface fields, thus increasing the probability of vacuum arcs or "breakdowns".

Breakdowns lead to random beam kicks that can result in emittance growth or even loss of the beam if the kick is strong enough. When applying the spot scanning technique to the dose delivery, beam losses lead to unacceptable "cold spots" in the dose distribution [6]. A high *Break-Down Rate* (BDR) (that is the fraction of the RF pulses in which there is a break-down) deteriorates also the linac vacuum and can compromise the reliability of the machine.

A series of high RF power, single-cell experiments have been performed in order to quantify the high gradient operation limitations of 3.0 and 5.7 GHz structures. Both frequencies lead to compact RF structures which still have practical dimensions for fabrication.

The experiments aimed at:

1. measuring the BDR at field levels in the operation range of hadron therapy linacs: above 170 MV/m of surface electric field for 3 GHz and 200 MV/m for 5.7 GHz.
2. determining the scaling laws that relate breakdown rate, pulse length, electric field and modified Poynting vector (which is used to quantify this effect as discussed in [7]) and compare the results with data available for 11.4–12.0 GHz and 30.0 GHz structures [7].

This paper presents the design choices for the cavity test prototypes [8], describes the test setups and discusses the BDR measurements with respect to the major electromagnetic quantities. In the last Sections the results are compared with high-gradient results of structures operating in different frequency bands.

2. Design and prototyping of test cavities

Hadrontherapy typically uses proton beams with energies between 70 and 230 MeV and carbon ion beams with energies between 120 and

* Corresponding author.
E-mail address: alberto.degiovanni@alumni.epfl.ch (A. Degiovanni).
[1] Present address: A.D.A.M. SA, rue de Veyrot 11, CH-1217 Meyrin, Switzerland.
[2] Present address: CERN, CH-1211 Geneva, Switzerland.
[3] Present address: Brookhaven National Laboratory, Upton, NY 11973, USA.

https://doi.org/10.1016/j.nima.2018.01.079
Received 16 October 2017; Received in revised form 22 January 2018; Accepted 23 January 2018
Available online 9 February 2018
0168-9002/

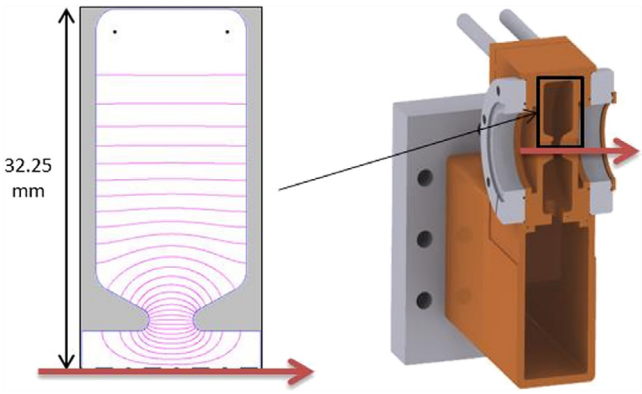

Fig. 1. Inner shape of the S-band (3 GHz) cell structure. The electric field lines are visible in the left figure obtained from simulations with the code Superfish.

430 MeV/u. This corresponds to a relativistic beta in the range 0.4–0.7. The most efficient and stable linac option for such range of energies is the so-called Cell Coupled Linac (CCL) structure in the form of a side coupled linac [9].

A CCL structure consists of a bi-periodic array of RF cells coupled together. Accelerating cells are placed on-axis and provide the longitudinal electric field needed for acceleration of the beam. Coupling cells are off-axis and are used to couple the electro-magnetic field between accelerating cells. A CCL structure works in the $\pi/2$ mode, which is the most stable mode with respect to frequency errors; on the other hand, the beam just sees a phase advance of 180° between the centers of two successive accelerating gaps. This feature allows optimizing the accelerating cells to maximize their shunt impedance and achieve higher acceleration efficiency than a Drift Tube Linac (DTL).

Two test prototypes, having similar layouts, have been designed and built to test their high gradient limitations: one operating at 3 GHz (S-band) and the other at 5.7 GHz (C-band).

A prototype consists of a single-cell cavity operating in the TM_{010} mode. The cavity is fed by a waveguide through a coupling slot opened on the rim of the cell. The main scope of the tests is to achieve the highest possible field inside the structure with the available RF power supplies. The simple layout of the test prototypes was chosen to satisfy this purpose.

The inner geometry of the single cell is the same as the one for the accelerating cells of one of the linacs designed by the TERA Foundation. The cell geometry was designed to maximize the shunt impedance. As the shunt impedance decreases with the bore hole aperture, the bore hole aperture was chosen taking as a reference proposed linac designs [2,3]. The cell geometry is shown schematically in Fig. 1. The length of the S-band test prototypes was chosen to be equivalent to a cell with a synchronous beta of 0.378 (or equivalently for proton at 75 MeV). The C-band test prototype had a similar length, but given the frequency ratio, the synchronous beta was 0.716 (or equivalently for fully stripped carbon ions at 405 MeV/u). The two protrusions close to the axis, called "nose cones" or just "noses", have the purpose of enhancing the field along the axis and thus increasing the transit time factor. The presence of such noses is a specific feature of low and medium beta accelerating copper structures.

Both test prototypes are made of UNS (Unified Numbering System) C10100 Oxygen-Free Electronic (OFE) copper alloy. The cavities were produced by VECA (Italy). The surface arithmetical-mean roughness (Ra) requested for manufacturing was 0.4 μm. The machining tolerance band was 20 μm for the 3.0 GHz cavity and 10 μm for the 5.7 GHz cavity. The two cavities were cleaned (degreasing, pickling and passivation) at CERN (Switzerland) and vacuum brazed at Bodycote (France). The test cavities were equipped with cooling channels in order to dissipate the RF power and to stabilize the cavity temperature during operation.

Table 1
Main electromagnetic quantities for the S-band and C-band test structures.

Structure	S-band	C-band
RF frequency [GHz]	2.998	5.712
Cell length [mm]	18.9	18.8
Cell diameter [mm]	64.50	34.54
Bore hole radius [mm]	3.5	1.5
Quality factor	9140	8500
Shunt impedance [MΩ/m]	83.3	98.7
Transit time factor	0.893	0.905
Synchronous beta	0.378	0.716
E_{max}/E_0	6.5	4.6
H_{max}/E_0 [kA/MV]	2.96	3.10
sqrt($S_{c,max}$)/E_0 [sqrt (MW/mm^2)/(MV/m)]	0.032	0.025

The 3.0 GHz cavity was tuned by deforming the nose region from the outside on both sides of the bore hole with a bar clamp. By reducing the gap length, or distance between the noses, the resonant frequency of the cavity decreased. The tuning of the 5.7 GHz test cavity was performed in successive steps by reducing the height of the tuning rings of the cell. The design, fabrication and low power RF measurements of the test cavities are fully described in [10,11].

Fig. 2 shows the distribution of the electric, magnetic and modified Poynting vector fields in the cell volumes of the 3.0 and 5.7 GHz test cavities. The modified Poynting vector S_c, introduced in Ref. [7], is defined by the equation:

$$S_c = \mathrm{Re}\{S\} + g_c \cdot \mathrm{Im}\{S\} \quad (1)$$

where $g_c = 1/6$ and S is the "classic" Poynting vector.

The peak value of electric, magnetic fields and modified Poynting vector – respectively, E_{max}, H_{max} and $S_{c,max}$, – are all located on the cell noses.

The quantities E_{max}/E_0, H_{max}/E_0 and $sqrt(S_{c,max})/E_0$ describing the ratio between the peak surface fields and the average axial electric field E_0, were computed with HFSS simulations. Their values are listed in Table 1, together with other relevant geometric and electro-magnetic quantities.

3. High power test setup

The 3 GHz prototype tests were conducted at the CERN CLIC Test Facility (CTF3). The test setup is shown in Fig. 3.

The S-band structure was connected, through a WR284 waveguide network, to a 35 MW peak-power klystron. A bi-directional coupler installed before the structure allowed measuring forward and reflected power signals. The beam line on one side of the cavity was connected to few diagnostics elements: a Faraday cup (to measure the field emitted current), and a photomultiplier (to detect light sparks during breakdown events). Breakdown detection was automatic, based on the detection of a peak in the reflected signals and of current bursts measured with the Faraday cup (see Section 4).

The 5.7 GHz cavity test was conducted at the test facility of A.D.A.M. SA at CERN. The cavity was fed by a 2.5 MW magnetron (Fig. 4). A 2.5 m-long WR187 waveguide network connected magnetron and cavity. The RF line included a circulator to revert the possible reflected power away from the magnetron. The cavity vacuum was isolated by a commercial RF window. Forward and reflected power signals were extracted from a directional coupler installed 0.5 m upstream of the cavity. A Faraday cup and a photomultiplier were used to identify breakdowns.

4. Measurements and results of the high-power tests

The two structures were conditioned for few days according to a specified procedure: the pulse length was increased step by step at low power level and then the power was ramped up to the maximum value.

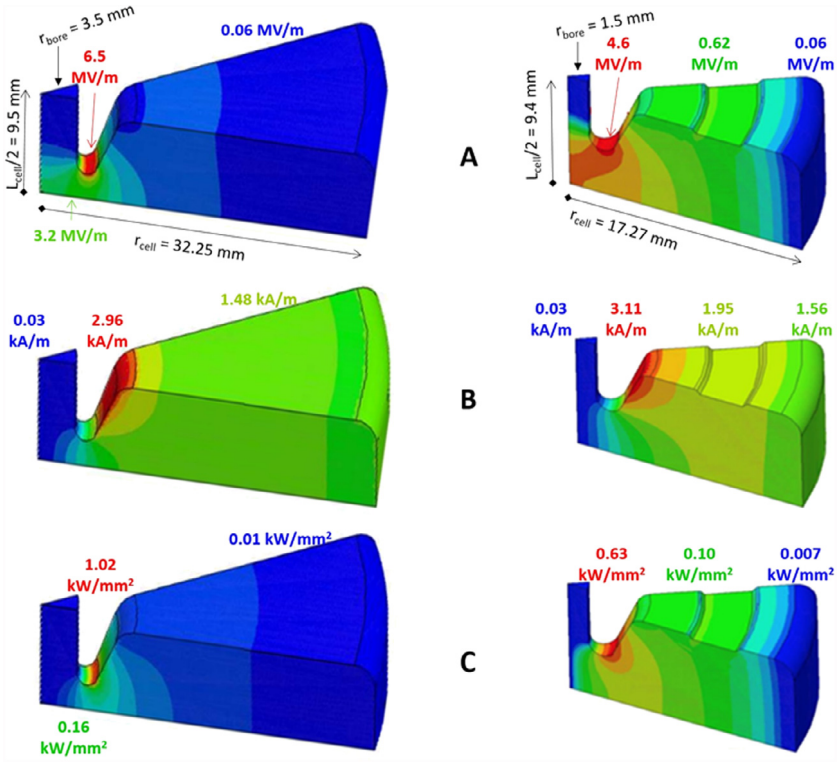

Fig. 2. Distribution of electric (A), magnetic (B) and modified Poynting vector (C) fields normalized to an axial field E_0 of 1 MV/m in the cells of the 3.0 GHz (left) and 5.7 GHz (right) test cavities from HFSS simulations.

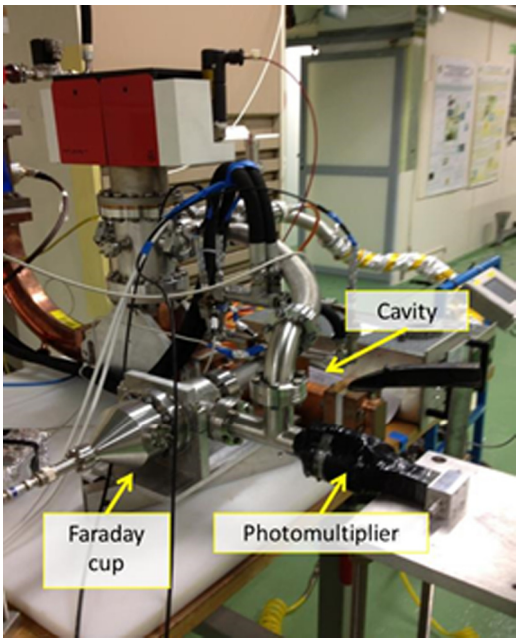

Fig. 3. Setup of the 3 GHz test stand at CTF3.

This is the same approach used for the conditioning of CLIC accelerating structure as described in [12]. Breakdowns were identified both from the sudden increase in reflected power within the same RF pulse and from the current burst seen in the Faraday Cup and photomultiplier. An example of the typical recorded incident and reflected power signals for normal pulses and breakdown pulses are reported in Fig. 5. A detailed

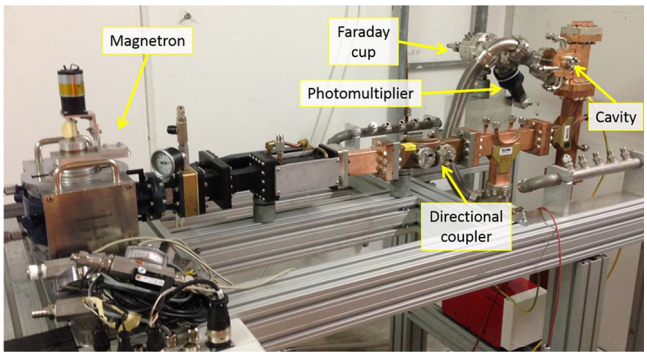

Fig. 4. Setup of the 5.7 GHz test stand at the laboratories of A.D.A.M. SA.

discussion and presentation of the data collected during the tests can be found in [11,13].

A summary of the history of the breakdown measurements is presented in Table 2. The number of pulses used to accomplish the conditioning (R2) of the C-band cavity was smaller than for the S-band cavity. Due to the smaller bore hole aperture radius (1.5 mm compared to 3.5 mm), the surface of the nose cones – calculated from the 3D model as the area with a slope and the two rounding angles – of the C-band cavity is smaller with respect to the S-band cavity (R4), that is, the C-band cavity has a smaller surface where breakdown nucleation sites can be found. If this difference is taken into account, the results collected in Table 2 indicate that the breakdown obtained during conditioning and evaluated per unit surface (R5) was comparable in the two tests.

The breakdown rate *BDR* is the magnitude that quantifies the number of breakdowns N_{bd} observed during the operation of an RF structure, where N_{pulses} is the number of RF pulses sent to the structure during the measurement. The BDR is measured in "breakdown per pulse"

Table 2
Summary of BDR measurements on S-band and C-band structures.

		S-band	C-band
R1	Total number of pulses [$\times 10^6$]	55.5	38.1
R2	Number of pulses during conditioning [$\times 10^6$]	33	28
R3	Number of breakdowns during conditioning [$\times 10^3$]	20	8.5
R4	Nose cone surface [mm^2]	316	144
R5	Number of breakdowns per surface unit during conditioning [$\times 10^3/mm^2$]	0.063	0.059
R7	Number of pulses with $E_s < 280$ MV/m [$\times 10^6$]	17.1	8.9
R8	Number of pulses with $280 < E_s < 320$ MV/m [$\times 10^6$]	3.3	1.7
R9	Number of pulses with $E_s > 320$ MV/m [$\times 10^6$]	2.2	0.4

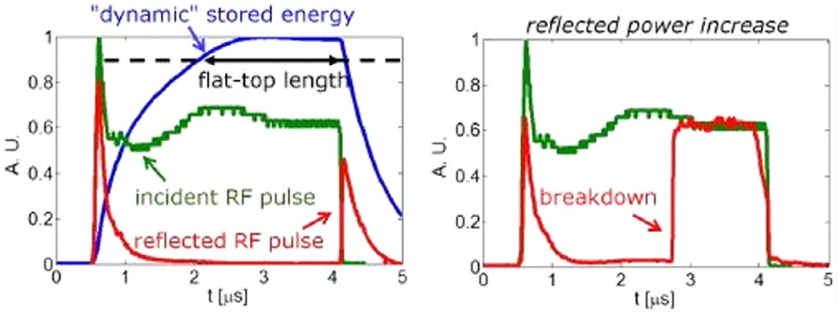

Fig. 5. Diagnostic signals: incident and reflected RF power amplitude for normal operation (left) and during a breakdown pulse (right) [11].

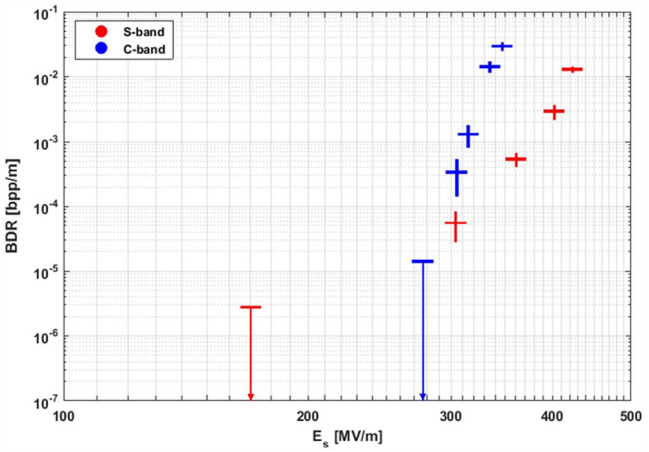

Fig. 6. Results of the BDR measurements obtained at different values of surface electric field E_s (in a double logarithmic scale plot) for a pulse duration equal to 2.1 us and 1.7 us respectively for the S-band and C-band cavities. The horizontal lines in the plot indicate the measured upper limits.

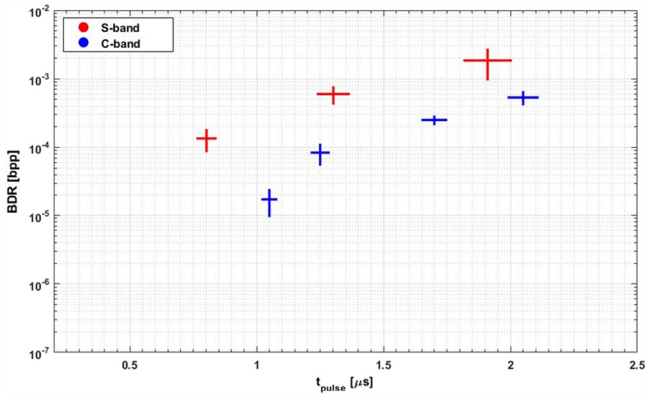

Fig. 7. Results of the BDR measurements obtained varying the pulse length at 3 GHz and 5.7 GHz, at constant surface electric field of 400 MV/m and 320 MV/m respectively.

(bpp). Sometimes it can be useful to evaluate the "BDR per unit length" (measured in bpp/m), which is obtained by normalizing the BDR to the cell length L_{cell}.

$$\text{BDR [bpp/m]} = \frac{N_{bd}}{N_{pulses} \cdot L_{cell}[\text{m}]} \tag{2}$$

The BDR measurements were performed during the last days of each one of the two tests. These measurements were performed at fixed pulse length and different power level, in order to obtain the dependence of BDR on the maximum surface field E_s achieved in the cavity. Fig. 6 shows a summary of the two sets of measurements performed with a RF pulse duration equal to 2.1 us and 1.7 us respectively for the S-band and C-band cavities.

No pick-ups were used to directly measure the field inside the cavity in order to avoid possible breakdown enhancements. The peak surface field excited in the cavities was calculated from the input power sent to the cavity using simulation results from HFSS (Table 1). The calibration of the RF circuit led to an uncertainty in the power value of about 10%. Thus in Fig. 6 a 5% error is assigned to the surface electric field. The uncertainty on the BDR takes into account the statistical error associated with the breakdown event counts, which was assumed to follow a Poisson distribution. The uncertainty is thus given by the square root of the measured number of events.

No breakdown event was detected during the time allocated for the lowest field measurements for both 3 GHz and 5.7 GHz cavities (respectively 19.1 and 3.8 million pulses). The BDR values reported for the lowest field correspond to one event.

The results of another set of measurements, performed at fixed value of the surface electric field and for different values of the pulse length, are shown in Fig. 7. The surface electric fields were 400 MV/m and 320 MV/m at 3 GHz and 5.7 GHz respectively.

5. Analysis and discussion

Previous results of extensive experimental data collected at 11.4 and 30.0 GHz showed that BDR, peak surface electric field E_s and RF

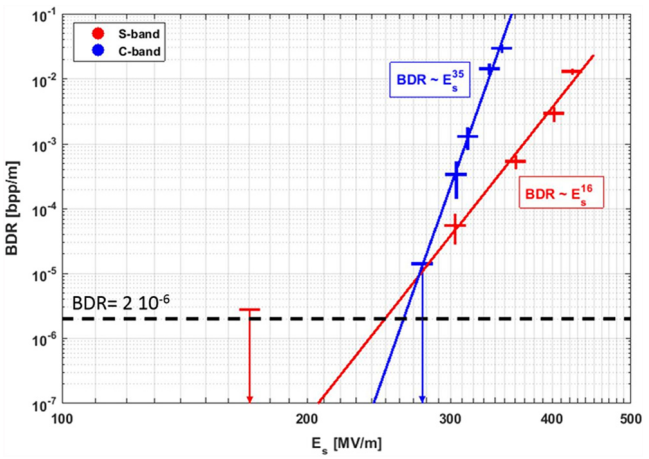

Fig. 8. BDR measurements with fits to scaling law in Eq. (3). The dashed line represents the maximum BDR allowable for reliable operation of a cyclinac for hadrontherapy applications. The BDR values reported for the lowest field represent an upper limit on the BDR. (For interpretation of the references to color in this figure legend, the reader is referred to the web version of this article.)

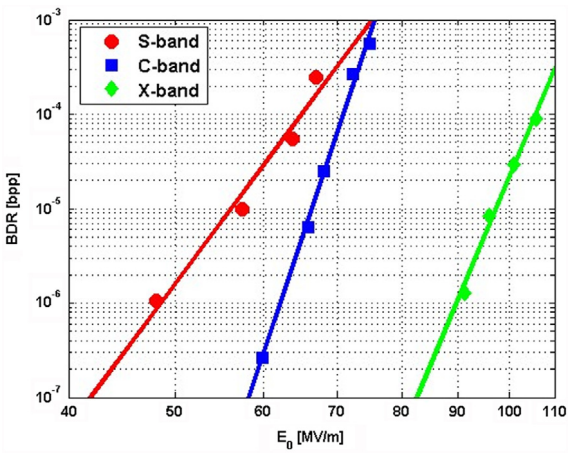

Fig. 9. BDR with respect to average axial field at different frequencies rescaled to pulse length of 2 us.

pulse width or pulse length t_{pulse} are linked through a scaling law of the type [7]:

$$\frac{E_s^x t_{pulse}^y}{\mathrm{BDR}} = \text{constant} \tag{3}$$

Other quantities, apart from the peak surface field E_s, have also been considered related to RF breakdowns and BDR. In particular the peak surface magnetic field H_s, the peak modified Poynting vector S_c, and the temperature increase due to pulsed surface heating $dT_{p.h.}$ [14].

Fig. 8 shows the fit of the scaling law in Eq. (3) to the measured data points for constant pulse length.

The dependence of BDR on the electric field, according to the power law in Eq. (3), gives a large exponent for the C-band structure, equal to 35 ± 11. Such large uncertainty has to be attributed to the small range of fields that could be tested as consequence of the limited test time. At 3 GHz the error is much smaller: 16 ± 5.

These results are listed in the second and third column of Table 3, together with the parameters y which quantifies the dependence on the duration of the RF pulse. The corresponding uncertainty was estimated as follows. For each data point a set of ten thousand values was generated randomly starting from a normal distribution with mean equal to the average value of the data point and standard deviation equal to the estimated BDR error for that data point. For each of the ten thousand sets a fit was obtained. The standard deviation of the set of fit parameters is taken as error on the mean fit parameter.

The last column of Table 3 indicates the average values measured on tests performed at 11.4, 12.0 and 30.0 GHz reported in [7,15] and reference therein.

It is seen that the parameters y and x do not vary, within large errors, between 5.7 and 30 GHz, while they are about twice smaller at 3 GHz.

Unfortunately, only few data of high gradient experiments at 3.0 GHz are available, so it is difficult to compare the S-band test results with former studies. Most 3 GHz structures are RF guns where cathode surface fields in the order of 140 MV/m are typically reached with very low breakdown rate (less than 10^{-8} bpp) [16] values which are compatible with an extrapolation of the red line of Fig. 8.

The power law found for the C-band test can be compared instead with the high gradient test of the Frascati C-band TW structure for the SPARC project [11]. The fit of the type BDR ~ E^x to the data points measured during that test gave as result a value of $x = 35 \pm 5$, in agreement with the data listed in Table 3.

5.1. Implications for medical hadron linacs

Which are the implications of these results for medical hadron linacs?

A BDR value of $2 \cdot 10^{-6}$ bpp/m can be considered here as a limit for ensuring reliable operation because, for a 20 m-long linac working at 200 Hz, it corresponds to a mean time between BD larger than 120 s, which is the typical delivery time of a fraction in proton therapy treatment. As seen in Fig. 8, the maximum surface field to achieve a BDR of $2 \cdot 10^{-6}$ bpp/m can be obtained by extrapolating the data with the two fits. The BDR limit of $2 \cdot 10^{-6}$ bpp/m is reached for surface fields larger than 250 MV/m at 3 GHz and 260 MV/m at 5.7 GHz. For the two prototypes and the typical CCL structures designed by the TERA Foundation, they correspond to average maximum gradients equal to 38 MV/m and 56 MV/m respectively. The peak electric surface field was not taken into account when optimizing the geometry of the S-band cavity. This could be done in further developments when very high gradients are desired at the expense of an increased power consumption.

5.2. Comparison of BDR measurements at different frequencies

Eq. (3) can be used to scale the results of BDR measurements to a reference electromagnetic quantity and to a reference pulse length. This has been done to compare the BDR measurements for the S-band and C-band tests to the results of a 11.4 GHz single-cell standing wave structure tested in SLAC [17]. Fig. 9 shows the BDR measured at different frequencies as a function of the average axial electric field E_0 and scaled to a pulse length of 2.0 us. Higher accelerating fields are achievable at higher frequencies, but in this case, it is important to remember that the geometries considered are different and the results could be biased by the fact that the synchronous beta is different in the three cases (i.e. 0.378, 0.716 and 1.0 for the S-band, C-band and X-band respectively) and increasing with frequency.

The four plots of Fig. 10 show the measured BDR as a function of peak surface electric field E_s (top left), peak surface magnetic field H_s (top right), peak modified Poynting vector S_c (bottom left) and temperature increase due to pulsed surface heating $dT_{p.h.}$ (bottom right) for the three considered frequencies (red: 3 GHz, blue: 5.7 GHz and green: 11.4 GHz). All BDR measurements are scaled to a reference pulse length of 2 us using the pulse length dependence expressed in Table 3. The value of g_c appearing in the definition of the Poynting vector, was assumed to be frequency-independent and equal to 1/6.

The modified Poynting vector is the quantity for which the spread of the data is minimum, meaning that the model behind it describes much better than the others the BDR limit in the large frequency range that goes from 3 to 30 GHz.

Table 3
Summary of the results of BD at different frequencies. S-band and C-band results were measured during the tests described in this paper, X- and K-band results are extracted from literature.

		S-band	C-band	X & K-band
RF frequency [GHz]		3.0	5.7	11.4 & 30.0
Pulse length dependence BDR $\sim t_{pulse}^{y}$ at fixed field	$y =$	2.9 ± 0.5	4.9 ± 1.2	5 ± 1
Peak field dependence BDR $\sim E_s^x$ at fixed pulse length	$x =$	16 ± 5	35 ± 11	30 ± 8

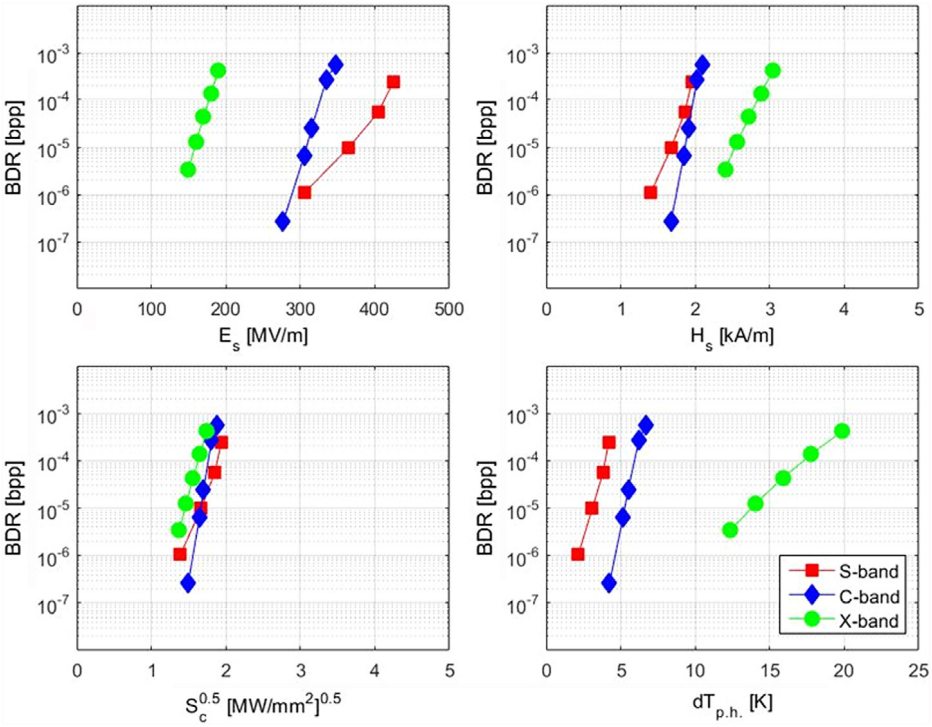

Fig. 10. Results of BDR measurements at different frequencies rescaled to the same pulse length of 2.0 us and with respect to several field quantities that can be responsible for breakdown effects, like peak surface electric field E_s (top left), peak surface magnetic field H_s (top right), peak modified Poynting vector S_c (bottom left) and temperature increase due to pulsed surface heating $dT_{p.h.}$ (bottom right). (For interpretation of the references to color in this figure legend, the reader is referred to the web version of this article.)

6. Conclusions

Accelerating gradients used in normal conducting electron linacs are typically around 15 MV/m. The extensive set of BDR measurements, performed on high frequency medium-beta structures (3.0 and 5.7 GHz) and described in this paper, aimed at determining the largest accelerating gradients that can be reliably obtained in high frequency copper structures for protons and light ions, thus allowing to reduce size and cost of hadron therapy linacs.

The tests performed by TERA indicate that linacs for hadron therapy working at S-band and C-band can be operated at surface electric fields of about 250 MV/m with a BDR smaller than $2 \cdot 10^{-6}$ bpp/m (equivalent to less than one breakdown per treatment session in a 20 meter-long linac working at 200 Hz). This limit corresponds to maximum gradients of 38 MV/m at 3.0 GHz and 56 MV/m at 5.7 GHz for the presented cavity geometries (with peak electric surface field to gradient ratios of 6.5 and 4.6 respectively).

Based on these results, a traveling wave linac structure at 3.0 GHz has been designed and built to test the possibility to achieve even higher gradients with optimized shape of the "noses" [18]. Furthermore, an optimized design at 9.3 GHz can also be envisaged, in order to understand whether increasing the frequency could allow for even higher accelerating gradients.

By comparing the results of the tests with higher frequency literature data it has been concluded that the modified Poynting vector model of Ref. [7] describes the BDR behavior of high gradient structures in a large range of frequency, from 3 to 30 GHz.

Acknowledgments

The authors would like to express their gratefulness to the CTF3 group for technical and scientific support to prepare and perform the experiment and to the CLIC RF structure development group for the enriching discussions about the preparation, development and analysis of the test. A special thanks to Walter Wuensch, Igor Syratchev and Alexej Grudiev for passionate discussion and deep insight at different stages of the high-gradient test program. The help of A.D.A.M. SA in setting up the measurement at 5.7 GHz is also acknowledged. Special thanks go to Luca Timeo for the extensive contributions during the cavity frequency tuning and test preparation and to Alexey Dubrovskiy, Eugenio Bonomi, Ben Woolley and Joseph Tagg for the help and continuous support with the control and acquisition system used during the high-power tests.

We are grateful to Vodafone Italy foundation for the funding received to fabricate the test cavities and for the support of some of the participants. The research leading to these results was partially funded by the Seventh Framework Programme [FP7/2007–2013] under grant agreement no. 215840-2.

References

[1] PTCOG, http://www.ptcog.ch/index.php/patient-statistics/, last accessed on 09.08.2017.

[2] A. Degiovanni, U. Amaldi, D. Bergesio, C. Cuccagna, A. LoMoro, P. Magagnin, P. Riboni, V. Rizzoglio, Design of a fast-cycling high-gradient rotating linac for protontherapy, in: Proc. of International Particle Accelerator Conference - IPAC13, 2013, pp. 3642–3644, Shanghai (China).
[3] S. Verdú-Andrés, U. Amaldi, A. Faus-Golfe, CABOTO, a high-gradient linac for hadrontherapy, J Radiat Res. 54 (Suppl 1) (2013) i155–61. http://dx.doi.org/10.1093/jrr/rrt053.
[4] U. Amaldi, P. Berra, K. Crandall, D. Toet, M. Weiss, R. Zennaro, E. Rosso, B. Szeless, M. Vretenar, C. Cicardi, C. De Martinis, D. Giove, D. Davino, M.R. Masullo, V. Vaccaro, LIBO-a linac-booster for protontherapy: Construction and test of a prototype, Nucl. Instrum. Methods A 521 (2004) 512–529.
[5] C. De Martinis, D. Giove, U. Amaldi, P. Berra, K. Crandall, M. Mauri, M. Weiss, R. Zennaro, E. Rosso, B. Szeless, M. Vretenar, M.R. Masullo, V. Vaccaro, L. Calabretta, A. Rovelli, Acceleration tests of a 3 GHz proton linear accelerator (LIBO) for hadrontherapy, Nucl. Instrum. Methods A 681 (2012) 10–15.
[6] U. Amaldi, S. Braccini, P. Puggioni, High Frequency Linacs for Hadron- Therapy. Review of Accelerator Science and Technology - RAST, Vol. II, World Scientific, 2009.
[7] A. Grudiev, S. Calatroni, W. Wuensch, New local field quantity describing the high gradient limit of accelerating structures, Phys. Rev. ST Accel. Beams 12 (2009) 102001; Phys. Rev. ST Accel. Beams 14 (2011) 099902 (erratum).
[8] A. Degiovanni, U. Amaldi, R. Bonomi, M. Garlasché, A. Garonna, S. Verdú-Andrés, R. Wegner, TERA high gradient test program of RF cavities for medical linear accelerators, Nucl. Instrum. Methods A 657 (2011) 55–58.
[9] T.P. Wangler, Principles of RF Linear Accelerators, John Wiley& Sons, 1998.
[10] R. Bonomi, Thermo-structural study and experimental analysis of accelerating structures for hadrontherapy linacs, (Ph.D. thesis), Politecnico di Torino, 2011.
[11] S. Verdú-Andrés, High-gradient accelerating structure studies and their application in hadrontherapy, (Ph.D. thesis), Universitat de València, 2013.
[12] A. Degiovanni, W. Wuensch, J. Giner-Navarro, Comparison of the conditioning of high gradient accelerating structures, Phys. Rev. Accel. Beams 19 (2016) 032001.
[13] A. Degiovanni, High gradient proton linacs for medical applications, (Ph.D. thesis) 6069, École Polytechnique Fédérale de Lausanne, 2014.
[14] D.P. Pritzkau, RF pulsed heating, (Ph.D. thesis), Stanford University, 2001 SLAC-Report-577.
[15] W. Wuensch, Progress in understanding the high-gradient limitations of accelerating structures, in: Proc. of APAC 2007, 2007, pp. 544–548, Indore, India, THYMA02.
[16] L. Faillace, Recent advancements of rf guns. proceedings of the workshop "physics and applications of high brightness beams: towards a fifth generation light source", Phys. Proc. 52 (2014) 100–109.
[17] V.A. Dolgashev, S.G. Tantawi, A.D. Yeremian, Y. Higashi, B. Spataro, Status of high power tests ofnormal conducting single-cell structures, in: Proc. of EPAC 2008, 2008, pp. 742–4, Genova (Italy), S LAC-PUB-15117.
[18] S. Benedetti, A. Degiovanni, A. Grudiev, W. Wuensch, U. Amaldi, RF design of a novel S-band backward travelling wave linac for proton therapy, in: Proc. of LINAC 2014, 2014, pp. 992-4, Geneva (Switzerland), THPP061.